— Final Report —

# Theory and Modeling of Petawatt Laser Pulse Propagation in Low Density Plasmas

PI: B. A. Shadwick

CO-PI: S. Y. Kalmykov

Award # DE-SC0008382

# All-Optical Control of Self-Injection

All-optical approaches to controlling electron self-injection and beam formation in laser-plasma accelerators (LPAs) were explored. It was demonstrated that control over the laser pulse evolution is the key ingredient in the generation of low-background, low-phase-space-volume electron beams. To this end, preserving a smooth laser pulse envelope throughout the acceleration process [1, 2, 4] can be achieved through tuning the phase and amplitude of the incident pulse [3, 11, 13, 16, 18, 20, 21]. A negative frequency chirp compensates the frequency red-shift accumulated due to wake excitation, preventing evolution of the pulse into a relativistic optical shock. This reduces the ponderomotive force exerted on quiescent plasma electrons, suppressing expansion of the bubble and continuous injection of background electrons, thereby reducing the charge in the low-energy tail by an order of magnitude [3, 16, 18, 20, 21]. Slowly raising the density in the pulse propagation direction locks electrons in the accelerating phase, boosting their energy, keeping continuous injection at a low level, tripling the brightness of the quasi-monoenergetic component [3]. Additionally, propagating the negatively chirped pulse in a plasma channel suppresses diffraction of the pulse leading edge, further reducing continuous injection. As a side effect, oscillations of the pulse tail may be enhanced, leading to production of low-background, polychromatic electron beams [16, 18, 20]. Such beams, consisting of quasi-monoenergetic components with controllable energy and energy separation, may be useful as drivers of polychromatic x-rays based on Thomson backscattering [21]. These all-optical methods of electron beam quality control are critically important for the development of future compact, high-repetition-rate, GeV-scale LPA using 10 TW-class, ultra-high bandwidth pulses and mm-scale, dense plasmas. These results emphasize that investment into new pulse amplification techniques allowing for ultrahigh frequency bandwidth, is as important for the design of future LPA as are the current efforts directed to increasing the pulse energy.

The radiation pressure of a multi-terawatt, sub-100 fs laser pulse propagating in an under-dense plasma causes complete electron cavitation. The resulting electron density "bubble" guides the pulse over many Rayleigh lengths, leaving the background ions unperturbed while maintaining GV/cm-scale accelerating and focusing gradients. The shape of the bubble, and, hence, the wakefield potentials, evolve slowly, in lockstep with the optical driver. This dynamic structure readily traps background electrons. The electron injection process can thus be controlled by purely optical means. Sharp gradients in the nonlinear refractive index produce a large frequency red-shift ($\Delta\omega \sim \omega_0$), localized at the leading edge of the pulse. Negative group velocity dispersion associated with the plasma response compresses the pulse into a relativistic optical shock (ROS). ROS formation slows the pulse (and the bubble), reducing the electron dephasing length and limiting energy gain. Furthermore, the ponderomotive force due to the ROS causes the bubble to constantly expand, trapping copious unwanted electrons, polluting the electron spectrum with a high-charge, low-energy tail. We have demonstrated a new, all-optical approach to compensating for the increase in pulse bandwidth, thereby delaying ROS formation and thus producing high quality, GeV-scale electron beams with 10-TW-class (rather than PW-class) lasers in mm-scale (rather than cm-scale), high-density plasmas ($n_{e_0} > 5 \times 10^{18}\,\mathrm{cm}^{-3}$ vs. $10^{17}\,\mathrm{cm}^{-3}$). We show that a negatively chirped drive pulse with an ultra-high ($\sim 400$ nm) bandwidth: extends the electron dephasing length; prevents ROS formation through dephasing; and almost completely suppresses continuous injection.

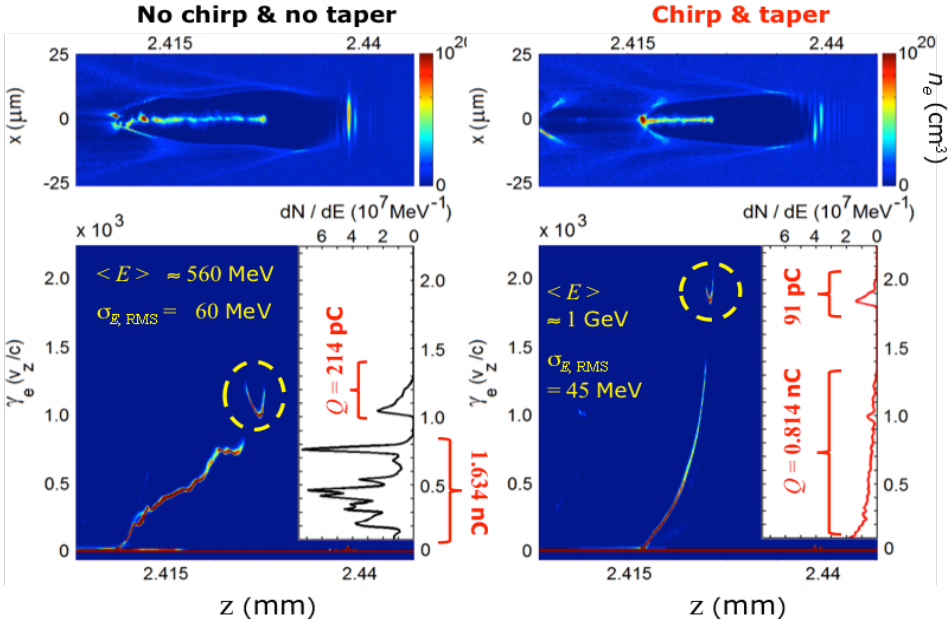


**Figure 1:** A 3-D PIC simulation (using CALDER-Circ) of electron acceleration through dephasing with 70 TW, 30 fs laser pulse [30]. Pulse propagates to the right. Negative frequency chirp gives the pulse a bandwidth corresponding to 5 fs transform-limited duration; the density taper corresponds to linear density variation from 0.8 to 1.2 of $n_{e_0}$, $n_{e_0} = 6.5 \times 10^{18}\,\mathrm{cm}^{-3}$. Combination of chirp and taper nearly doubles the energy and brightness of the quasi-monoenergetic component, allowing GeV energy gain over 1.8 mm distance (interval between injection and dephasing). At the same time, the low-energy tail is suppressed (factor 4 decrease in average flux).

We have also shown that a more precise compensation of the nonlinear frequency shift can be achieved using a higher-order chirp extracted from reduced simulation models. ROS formation can be further delayed by using a plasma channel to suppress diffraction of the pulse leading edge, minimizing longitudinal variations in the pulse. Plasma density tapering further delays dephasing, providing an additional boost in beam energy [13, 30, 34, 35].

An alternative method of eliminating the continuous injection, working especially well with PW lasers and low-density plasmas ($n_{e0} \sim 10^{17}\,\mathrm{cm}^{-3}$), uses the concept of a thin nonlinear plasma lens (NLPL). A thin dense plasma slab (then lens), placed before a multi-centimeter-length, low-density plasma (the accelerator), overfocuses an incident PW laser pulse at a controlled location inside the accelerator, creating an expanding electron density bubble that traps plasma electrons over a brief time interval. As soon as the balance between diffraction and nonlinear focusing is restored and self-guiding begins, the bubble transforms into the first bucket of an unbroken 3D electron plasma wave, thereby eliminating any chance for further injection. We have extended our original study of the NLPL concept, providing more detail on parameter optimization and examining sensitivity of the scheme to pulse aberrations [11].

Producing high-quality, GeV-scale electron beams with 1 J laser-pulses demands new ideas in photon engineering [7]. Maintaining GeV-scale electron energy at the 10 TW-scale pulse power requires raising the acceleration gradient to the 10 GV/cm level. Acceleration in the blowout regime, in dense, highly dispersive plasmas ($n_0 \sim 10^{19}\,\mathrm{cm}^{-3}$) naturally affords this gradient, with the added benefits of pulse self-guiding and electron self-injection. The feedback of the collective plasma motion onto the laser pulse, however, leads to evolution of the carrier frequency

and pulse envelope, leaving, in turn, its imprint on electron phase space. High-density plasmas rapidly compress the drive pulse, limiting the dephasing length, polluting the beam phase space with a broad-band population of electrons due to continuous injection; see Fig 3(a). Our results show that these effects can be avoided, and the self-injection process optimized, by using a drive pulse with an ultrahigh bandwidth (of the order of carrier wavelength). Introducing a negative frequency chirp helps compensate the nonlinear frequency red-shift imparted by the plasma response, thus mitigating pulse self-compression [3]. This method of optical control appear to be rather insensitive to the laser pulse phase; we have shown that this chirped driver need not be phase-coherent but can be synthesized by a superposition of transform-limited pulses with differing carrier frequencies. A piecewise negative chirp can be obtained by temporally advancing pulses with the higher carrier frequencies. In this scenario, the frequency-shifted pulses can be obtained from a conventional $0.8\,\mu\mathrm{m}$ oscillator, up-shifted in a Raman cell, and amplified by standard CPA techniques. Since all pulses originate from a single oscillator, precise synchronization of the pulses is possible. Our preliminary results [7], show that frequency shift, energy partition, and time delay among individual pulses provides ample freedom to control the acceleration process. We believe that this approach will scale to high repetition-rate with far less laser development effort than would be required for petawatt-class drivers and, in conjunction with pulse-shaping techniques, has the potential to deliver beam quality far superior to that offered by convention approaches.

Through the Thomson scattering mechanism, a comb-like electron beam can produce multi-

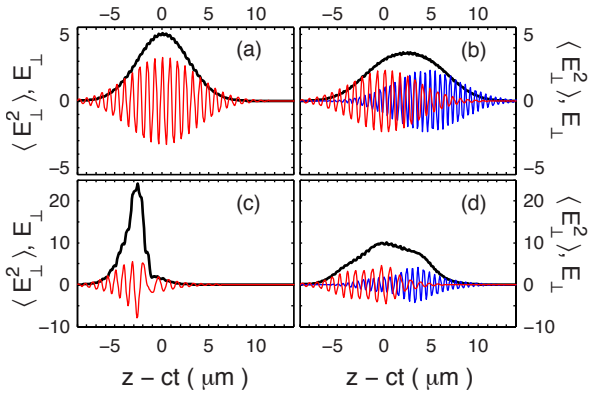


**Figure 2:** Evolution of synthesized broad-band pulses. Electric field of the pulse on axis (in units of $m\,\omega_0 c/e$): a transform-limited, $20\,\mathrm{fs}$ pulse with $\lambda = 0.8\,\mu\mathrm{m}$ (red) in a uniform plasma at $z = 0$, (a), and at full compression, $z = 1.6\,\mathrm{mm}$, (c); and two pulses, one with $\lambda = 0.8\,\mu\mathrm{m}$ and polarized in the $x$-direction (red) and the other with $\lambda = 0.53\,\mu\mathrm{m}$, polarized in the $y$-direction, and advanced by $15\,\mathrm{fs}$ (blue) at $z = 0$, (b), and at $z = 1.6\,\mathrm{mm}$, (d). The transform-limited pulse compresses significantly, while the synthesized broad-band pulse, propagating the same distance show little envelope deformation. The black line shows $E^2$ averaged over an optical cycle. The pulses propagate to the right. See Ref. [7].

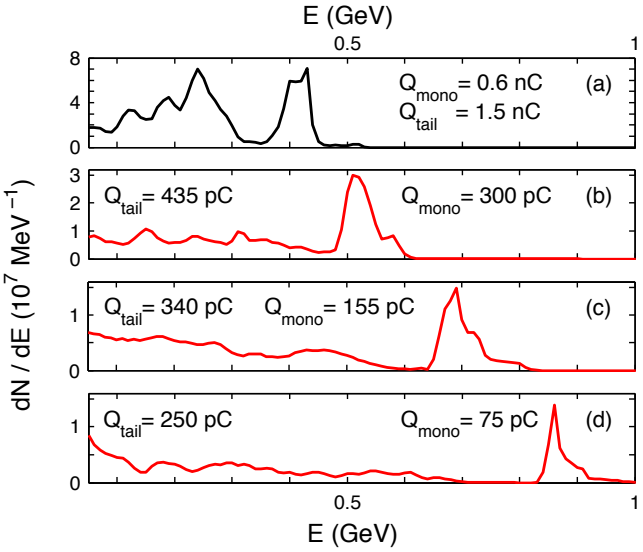


**Figure 3:** Controlling electron beam quality using a high-bandwidth driver. In each case, electron spectra are shown at dephasing. A transform-limited drive pulse ($20\,\mathrm{fs}$ and $1.4\,\mathrm{J}$) with $\lambda = 0.8\,\mu\mathrm{m}$ leads to significant dark-current: (a). Stacked drive pluses (each $20\,\mathrm{fs}$ and $0.7\,\mathrm{J}$) with $\lambda = 0.8\,\mu\mathrm{m}$ and $\lambda = 0.53\,\mu\mathrm{m}$ can optimized to dramatically improve beam quality: (b) no delay; (c) $10\,\mathrm{fs}$ delay and; (d) $15\,\mathrm{fs}$ delay (See Fig. 2). In spite of an 8-fold reduction in charge, the brightness of the quasi-monoenergetic component is increased by 60%.

color $\gamma$-rays [9, 10, 21, 23]. Figure 4(a.2)–(d.2) shows the photon flux per unit solid angle, in the direction of electron beam propagation (on-axis observation, $\theta = 0$), in the plane of the scattering laser pulse polarization resulting. [The electron beam phasespace is shown in Figure 4(a.1)–(d.1).] These figures demonstrate that reductions in the electron energy tail monochromatize the $\gamma$-ray signal. The photon energy bands in Figures 4(b.2)(d.2) are centered about $E_{ph} \approx 4\langle\gamma_e\rangle^2 E_{int}$, and have a sub-30% RMS energy spread owing to the mrad-scale electron beam divergence. These fs-length $\gamma$-ray beamlets of different colors have respective time delays on the order a few fs. Reducing the NCP length from 30 fs to 20 fs, while preserving the bandwidth and power, eliminates periodic injection, leaving a single QME feature dominant in both electron and photon spectra, with both electron and $\gamma$-ray flux significantly increased (see figures 7(a)).

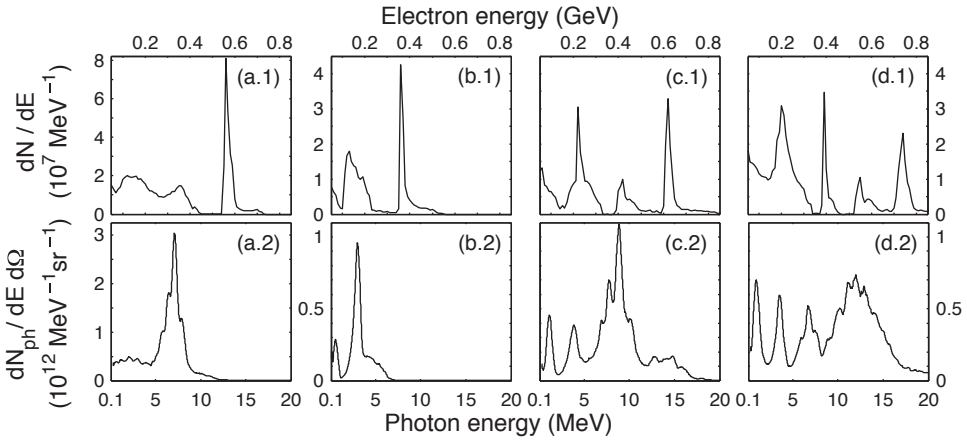


**Figure 4:** Energy spectra of mono- and polychromatic electron beams ((a.1)(d.1)) and ITS $\gamma$-rays ((a.2)(d.2)) in case 2 (a) and case 4 ((b)(d)). (a) z = 2.16 mm (dephasing), (b) z = 1.48 mm, (c) 2.08 mm, (d) 2.48 mm (dephasing). Statistics of electron beams at dephasing ((a.1) and (d.1)) are presented in Table 1. The photon flux in (a.2)(d.2) is taken on-axis, in the direction of electron beam propagation, and in the ILP polarization plane. See Refs. [9, 10].

# Advanced Numerical Methods

Extending our previous work [E. G. Evstatiev and B. A. Shadwick, J. Comput. Phys. **245**, 376 (2013)], we have developed a variational formulation of macro-particle models for electromagnetic kinetic plasma simulations [5, 6]. A self-consistent set of discrete macro-particle equations of motion are obtained from a discretized Lagrangian. Discretization of the Lagrangian was performed by reduction of the phase-space distribution function to a collection of finite-sized macro-particles of arbitrary shape, and subsequent discretization of the field onto a spatial grid. The equations of motion are then obtained by demanding the action be stationary upon variation of the particles and field quantities. This yields a finite-degree of freedom description of the particle-field system which is inherently self-consistent. The primary advantage of the variational approach relative to the more common Particle-In-Cell method is the preservation of the symmetries of the Lagrangian, which in our case leads to energy conservation and avoids difficulties with grid heating. Additional benefits originate from the decoupling of particle size from grid spacing and

a relaxation of the restrictions on particle shape, which leads to a decrease in numerical noise. The variational approach also guarantees a consistent level of approximation, and is amenable to higher-order approximations in both space and time.

As an example, consider the propagation of a laser pulse in an underdense plasma [6]. We take $\omega_0 = \omega_p$, laser dimensionless vector $a_0 = 0.5$ and pulse length $k_p\, L = 10$, and we use 10 macro-particles per cell. Figure 5 shows results with $k_p\, \Delta z = 0.025$, corresponding to 6001 grid points, and $c\, \Delta t = \Delta z/9$ and quartic $\rho_k$ using an RK4 integrator. Plotted in Fig. 5 are $q\, A_x/mc^2$ and $J_x/q\, n_0$ on the left axis and $N_e/n_0$ on the right axis at $\omega_p\, t = 0$ [panel (a)], $\omega_p\, t = 50$ [panel (b)], and $\omega_p\, t = 100$ [panel (c)]. As can be seen in the figure, the laser pulse is absorbed on the density transition, resulting in "surface" currents in the transition region, which subsequently re-radiate a left-going pulse as well as an evanescent wave [see Fig. 5(b) and (c)].

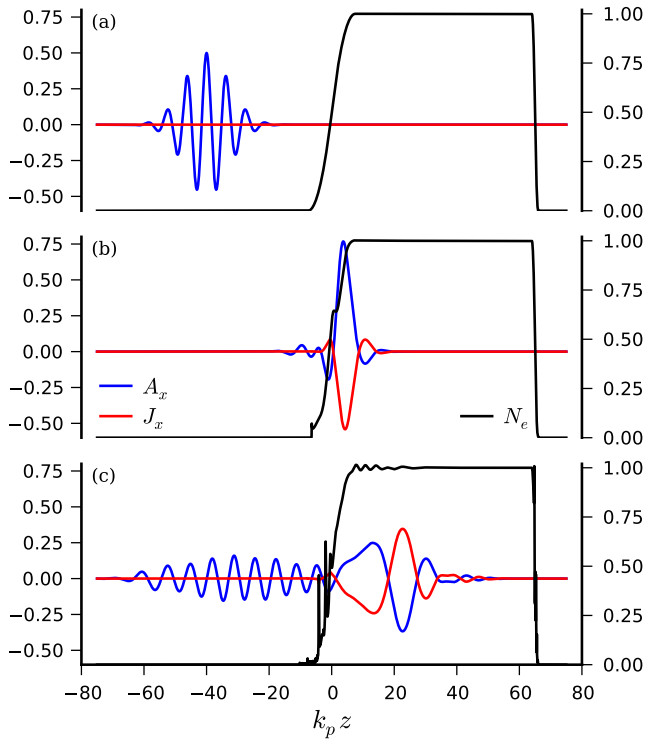


**Figure 5:** Laser pulse interacting with an overdense plasma at: (a) $\omega_p\, t = 0$; (b) $\omega_p\, t = 50$; and (c) $\omega_p\, t = 100$. The vector potential $q\, A_x/mc^2$ (red line) and transverse current $J_x/q\, n_0$ (blue line) are plotted on the left axis, while the macro-particle density $N_e/n_0$ (black line) is plotted on the right axis. The density shows the vacuum-plasma interface. See Ref. [6].

In the electromagnetic case, charge conservation plays an important role; gauge invariance and momentum conservation are both linked to charge conservation. In the presence of a spatial grid, a variational formulation cannot retain exact momentum conservation (and thus neither gauge invariance nor change conservation) as spatial translational symmetry has been broken. We have shown that in an average sense, summing over all macro-particles, charge is conserved [5]. As a result, we do not expect secular errors associated with the lack of exact (microscopic) charge conservation.

For many configurations of interest in laser-plasma interactions, it is computationally efficient to use a coordinate system co-moving with the laser pulse. Since we are using a Lagrangian formulation, we can easily transform to moving window coordinates yielding a particle algorithm explicitly formulated in the moving window. Thus we, for the first time, demonstrate an energy conserving set of discrete equations in moving window coordinates rigorously derived from a

discretized electromagnetic Lagrangian.

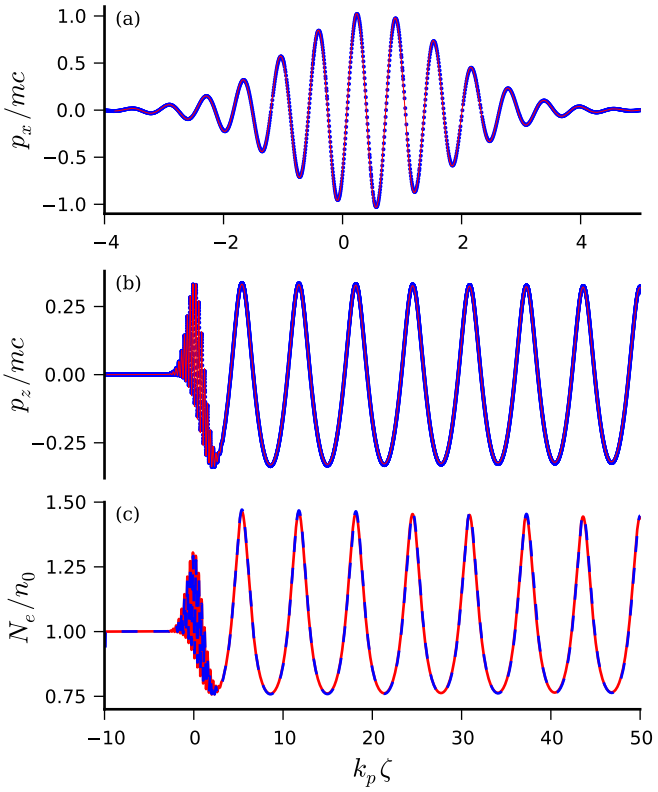


**Figure 6:** Comparison of our macro-particle model (blue) to the cold fluid model (red) of laser interacting with an under-dense plasma in moving window coordinates. Panels (a) and (b) show phase space at $\omega_p t = 60$ and panel (c) shows the normalized particle density $N_e/n_0$. In panel (a) we only show the area of non-zero $x$-momentum. See Ref. [6].

To provide an example of this method [6, 62], we consider an under-dense plasma with $\omega_0 = 10\,\omega_p$. The initial vector potential has dimensionless amplitude $a_0 = 1$ and pulse length $k_p\,L = 2$ (linear resonance). Boundary conditions are applied ahead of the laser pulse, i.e., the leading edge of the moving window encounters quiescent plasma, where we take the potentials and their derivatives to be zero. Our domain extends from $k_p\,\zeta_1 = -10$ to $k_p\,\zeta_2 = 70$ with 3201 grid-points ($k_p\,\Delta\zeta = 0.025$). We take $c\Delta\tau = \Delta\zeta$ and we use 8 particles per cell with a quartic particle shape. Figure 6 shows a comparison between our macro-particle calculation and the results of a cold fluid model. The fluid model, also formulated in the moving window, uses the same spatial differencing, time integration, grid parameters and initial conditions. Figure 6(a) shows the macro-particle transverse momentum (blue dots) overlaid on the transverse fluid momentum (red line). Likewise, Fig. 6(b) shows the macro-particle longitudinal momentum (blue dots) overlaid on the longitudinal fluid momentum (red line). Finally, Fig. 6(c) shows the macro-particle density (dashed blue line) and the fluid density (red line). There are no adjustable parameters in this comparison; the respective models used identical numerical parameters. Clearly the agreement is remarkable. The macro-particle model has virtually no noise, even in the density. No smoothing or filtering of any kind has been applied to the macro-particle results. Note also, there are no signs of grid-heating.

One significant advantage of the Lagrangian formulation is the ability to construct a (canonical) Hamiltonian representation by performing a Legendre transformation. This opens the door to using conventional symplectic integrations methods for the combined macro-particle and field phasespace. To illustrate the advantages of the symplectic integrator over the generic method, we

consider the problem of weak (linear) Landau damping where the wave-particle resonance occurs at velocities much greater than the thermal velocity [5, 62]. This is a particularly hard problem for a macro-particle method as only macro-particles in the tail of the distribution participate in the wave-particle resonance; the majority of the macro-particles are consigned to representing the thermal state and are not resonant. Since all macro-particles represent the same number of electrons, when only a small number of macro-particles are involved in the resonance, it is challenging to correctly capture the energy transfer from fields to particles (and thus the correct damping rate). Initially the plasma has a uniform density $n_0$ and is in thermal equilibrium with temperature $T_0$ satisfying $k_B\,T_0/mc^2 = 1/5$, where $k_B$ is Boltzmann's constant. We take periodic boundary conditions in space, a domain size of $L = 4\pi c/\omega_p$ spanning $1024$ cells, where $\omega_p = \sqrt{4\pi q^2 n_0/m}$ is the plasma frequency. These parameters were chosen to allow only a single weakly damped mode. The macro-particles are loaded in the center of the cell while the velocities are chosen randomly from a Gaussian distribution with variance $k_B T_0/mc^2$. At each spatial location, the macro-particle velocity distribution is shifted and scaled to have zero mean and variance exactly corresponding to $T_0$. The macro-particle spatial distribution $S$ is taken to be a two-cell wide tent-function, giving cubic $\rho_k$ for the corresponding expressions for $\rho_k$). Initially, we excite the $n = 2$ spatial mode of the electric field with initial amplitude $E_0$ given by $qE_0/(mc\,\omega_p) = 0.05$ by perturbing the macro-particle positions.

We provide an independent (and presumably more accurate) solution to this problem using an Eulerian Vlasov–Poisson solver known to have excellent conservation properties. We take identical initial conditions and spatial grid, a velocity grid spanning $-2 < v/c < 2$ with 401 grid-points with the distribution function vanishing at the limits of the velocity domain, and time-step $\omega_p \Delta t = 0.1$. With these parameters, the Vlasov–Poisson solution was sufficiently well converged that further refinements led to much smaller changes in this solution than the differences between this solution and any of the macro-particle solutions considered.

Figure 7 shows the amplitude of the $n = 2$ spatial Fourier mode of the electric field, $|\widetilde{E}_2|$, in units of $mc^2/q$ obtained from three methods [Vlasov–Poisson solver, (black); symplectic integrator, (red); and the Runge–Kutta integrator, (blue)], where the number of macro-particles is varied. Each panel is labeled with the number of macro-particles used at each point in space, $n_v$, to represent the velocity distribution. While the cases with $n_v = 400$ and $n_v = 800$ show disagreement between the Runge–Kutta and symplectic integrator solution, the discrepancies are not significant as they are smaller than the overall disagreement with the Vlasov solution. For $n_v = 1600$ (bottom), the macro-particle results closely track each other and the full kinetic solution through $\omega_p t = 30$ and give good qualitative agreement over the remainder of the evolution. Not only is this more macro-particles per cell than velocity grid-points used in the Eulerian method, the computational cost of the macro-particle solution is approximately 4 times greater than that of the fully-kinetic solution. (In all cases, the codes have been carefully optimized, so we believe this ratio reflects the intrinsic costs of the algorithms and is not significantly influenced by implementation details.) By further increasing $n_v$, it is reasonable to expect that the macro-particle solutions will exhibit better agreement with the Vlasov solution for $\omega_p\, t > 30$.

Figure 8 shows $|\widetilde{E}_2|$ in units of $mc^2/q$ obtained from the three methods [Vlasov–Poisson solver, (black); symplectic integrator, (red); and the Runge–Kutta integrator, (blue)], where $n_v = 1600$ and the value of $\Delta t$ used in the macro-particle integrators is varied. As the time-step is increased, the disparity between the symplectic integrator solution and the Vlasov solution increases only

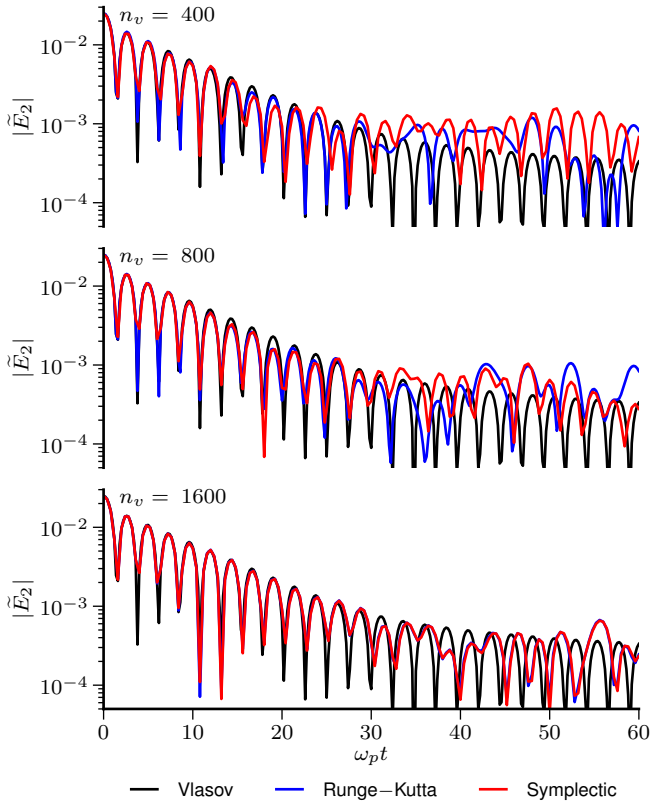


**Figure 7:** (Color online) Amplitude of the $n = 2$ spatial Fourier mode of the electric field in the weak Landau damping problem, computed with all three methods: Vlasov–Poisson solver, (black); symplectic integrator, (red); and the Runge–Kutta integrator, (blue). Each panel is labeled with the number of macro-particles, $n_v$, used at each point in space to represent the velocity distribution. The Vlasov–Poisson solution (black) is identical in all panels. In all cases, $\omega_p \Delta t = 0.1$ and the mode amplitude is plotted in units of $mc^2/q$. See Ref. [5].

slightly, whereas the Runge–Kutta integrator shows marked disagreement for $\omega_p \Delta t \geq 0.4$. This significant disagreement between the macro-particle methods is rather surprising since symplectic integrators are commonly held to be only strictly necessary when following a very large number of orbits; here we consider less than 10 plasma periods. It is likely that the energy behavior of the symplectic method (i.e., oscillation versus secular growth), more than its phase-space preserving properties, is responsible for the method's superior performance. Taking into account the relative sizes of $\Delta t$ needed by each method to give accurate solutions and the effort per time-step, the symplectic method is approximately 5–10 times more computationally efficient than the generic Runge–Kutta method.

We have worked to improve our implicit Vlasov solver and continued analysis of the algorithms. Discretizing phase space leads to a large coupled set of ordinary differential equation for the evolution of the distribution function and fields on the grid. Analysis of this discrete (but continuous time) system shows that total particle number, total momentum, total energy and $\int f^2 dx\, dv$ are exactly conserved. All other conservation laws of the Vlasov system are rendered approximate by the discretization of phase space. We integrate these equation in two different ways: 1) using the midpoint rule and 2) using a Strang-style operator splitting. The midpoint rule integrator respects all of the conservation laws that survive phase-space discretization. The difficulty with using the midpoint rule is the necessity to solve a (very large) nonlinearly coupled set of equations. For technical reasons, iterative methods are the only practical means of solution. The nature of the equations results in very slow convergence of the iterative solution. The Strang splitting approach is computationally far more attractive as it eliminates the need for an iterative solver but only approximately conserves energy. The phenomena of phase mixing and phase-space fil-

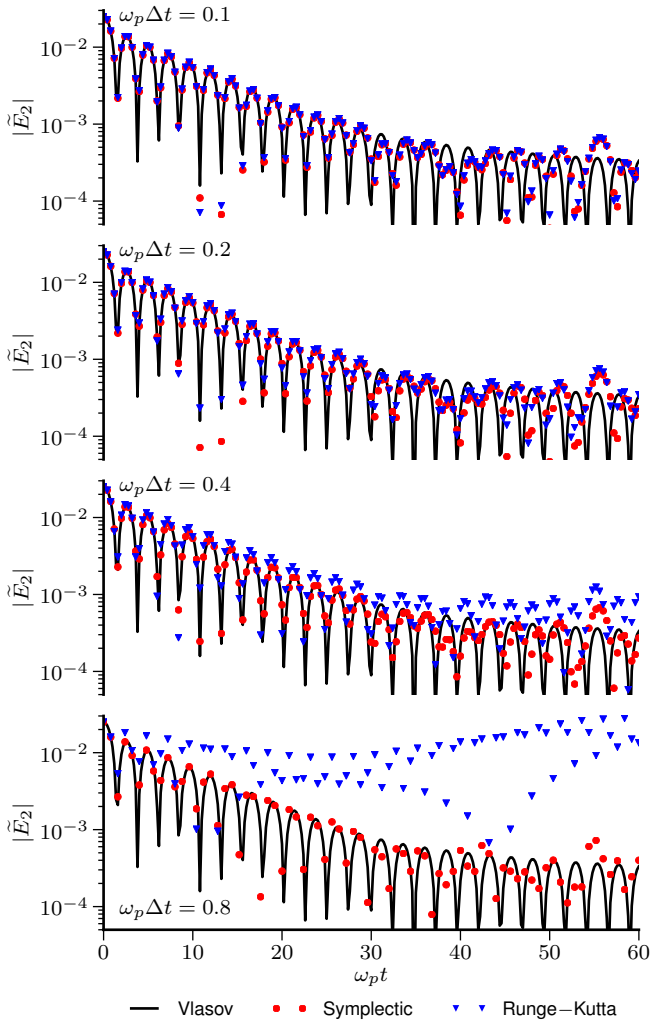


**Figure 8:** (Color online) Amplitude of the $n = 2$ spatial Fourier mode of the electric field in the weak Landau damping problem, computed with all three methods: Vlasov–Poisson solver, (black); symplectic integrator, (red); and the Runge–Kutta integrator, (blue). Each panel is labeled with the value of $\Delta t$ used by the macro-particle integrators in the computation. The Vlasov–Poisson solution (black) is identical in all panels and was computed with $\omega_p \Delta t = 0.1$. In all cases, $n_v = 1600$ and the mode amplitude is plotted in units of $mc^2/q$. See Ref. [5].

amentation makes the Vlasov equation numerically challenging. Absent collisions, filamentation proceeds unchecked to ever smaller scales, eventually reaching the grid scale where unphysical oscillations in the distribution function develop. Our algorithm, being free of numerical dissipation, can produce negative values of the distribution function. Flux limiters, originally developed for computational fluid dynamics, are commonly used to prevent such negative values. When applied to the Vlasov equation, we found flux limiters to have critical deficiencies: they force the time step to be small (so that flux is only deposited in a small number of adjacent cells in each time step); and they distort phase space and damage invariants. Conversely, negative values of the distribution function occur over small regions of phase space and give rise to neither of these deleterious effects.

We illustrate this behavior with the two-stream instability. Here, our implicit solver develops regions of negative density as phase-space filamentation develops. We consider both SMART and superbee flux-limiting algorithms. For comparison, we also solve the full nonlinear system with a Jacobian-free Newton–Krylov method. Fig. 9 shows the absolute value of the relative error in various invariants: (a) particle number, (b) total energy, (c) enstrophy, and (d) entropy produced by the different algorithms (split, unsplit, SMART, and superbee). Fig. 10 shows

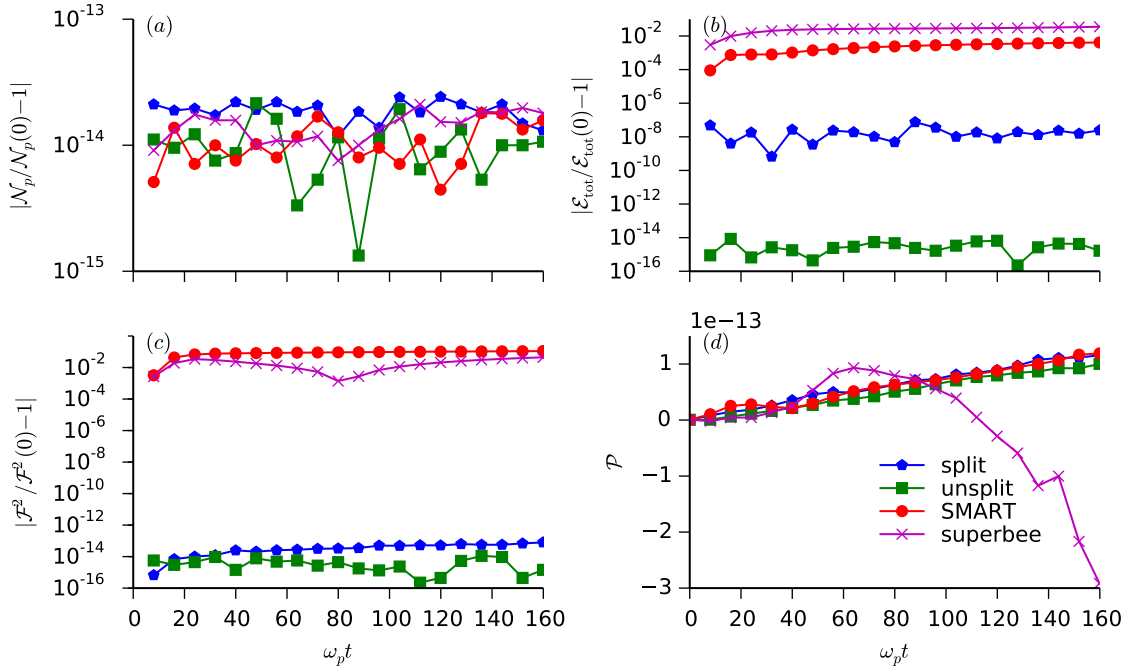


**Figure 9:** Conservation properties for the different algorithms (split, unsplit, SMART and superbee): (a) particle number, (b) total energy, (c) enstrophy absolute value of the relative error; and (d) total momentum.

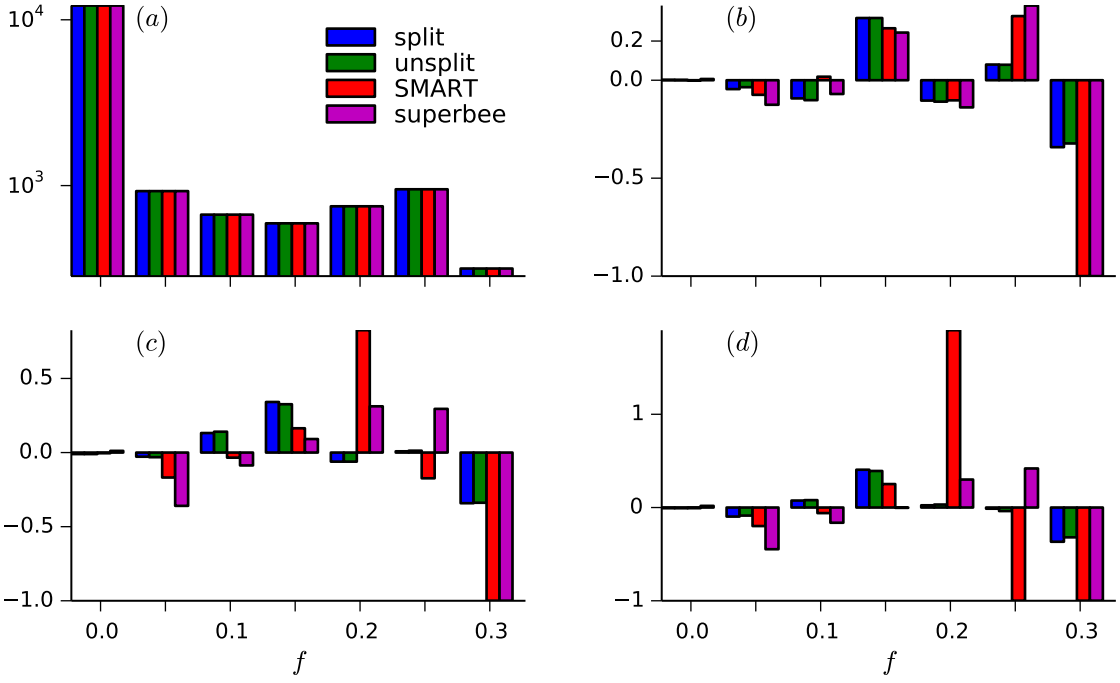


**Figure 10:** Phase-space volume partition of the distribution function for the three methods at different times of the simulation: (a) $\omega_p\, t = 0$, (b) $\omega_p\, t = 16$, (c) $\omega_p\, t = 40$, and (d) $\omega_p\, t = 80$.

histograms of the distribution function at different times; by Gardner's theorem, this histogram should be an invariant. Fig. 10(a) shows the histogram of the initial condition. Fig. 10(b)–(d) show relative changes in each bin at $\omega_p t = 16$, $\omega_p t = 40$, and $\omega_p t = 80$, respectively. The flux-limited algorithms perform poorly, the distribution function is progressively smeared out as filamentation develops. A manuscript is in the final stages of preparation and will be submitted presently. See also Ref. [33, 36, 46, 49].

In the Laplace transform treatment of the relativistic initial value problem, in addition to contributions to the electric field from poles (which give rise to the usual quasi-modes) there are contributions from branch cuts due to the upper bound on particle velocity. The asymptotic structure of the electric field due to these branch cuts was first determined by Godfrey et al. [B. Godfrey, B. Newberger, and K. Taggart, IEEE Trans. Plasma Sci. **3**, 185 (1975)] and later refined by Sartori and Coppa [C. Sartori and G. G. M. Coppa, Phys. Plasmas **2**, 4049 (1995)]. This behavior makes for a sensitive benchmark as the electric field must be followed for a large number of oscillations. This phenomena appears inaccessible to macro-particle methods as unmanageably large numbers of macro particles would be necessary to keep sampling noise low enough. To see this effect, it is necessary to chose $k$ and $T$ such that the quasi-mode solution is damped very rapidly and the branch cut contribution is non-negligible. To this end, we take $K = 8$, $T = 0.2\,mc^2$ and solve the linearised system of equations with $\omega_p \Delta t = 0.015$, $\Delta p = 0.005\,mc$ and $\omega_p \Delta x = 0.0245\,c$. For these parameters, the quasi-mode has $\omega_r = 7.903\,\omega_p$ and $\omega_i = -2.576\,\omega_p$ and thus decays rapidly. The amplitude of the electric field decays as

$$E \propto t^{1/6} \exp\left[-\frac{3\sqrt{3}}{4}\left(\mu^2 k\, c\, t\right)^{1/3}\right]. \tag{1}$$

The electric field from the numerical solution [8] is shown in Fig. 11 (blue line) along with amplitude given by (1) (red line). We see that very early in the calculation, the system enters the time-asymptotic behavior arising from the branch cut and there is excellent agreement between the numerical solution and the amplitude (1).

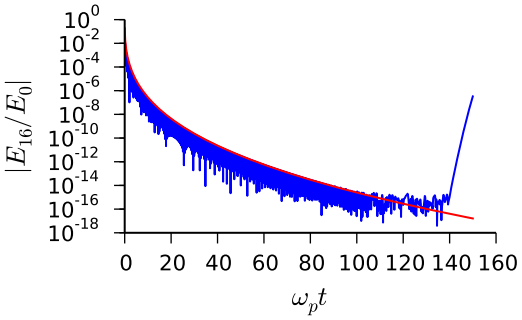


**Figure 11:** Electric field for $A = 0.1$, $kc/\omega_p = 8$ and $T/mc^2 = 0.2$ (blue) along with the amplitude given by (1) (red).

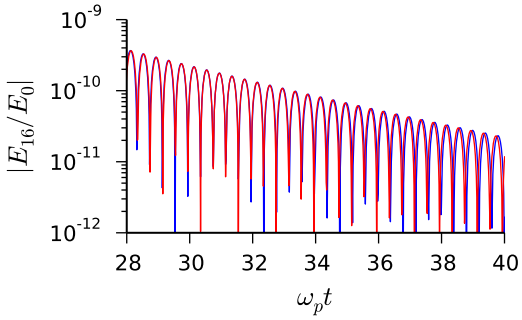


**Figure 12:** A comparison or the numerical solution (blue) with (2) (red). The section shown is representative of the electric field behavior over the full time interval.

Sartori provides a corrected expression for the full time-dependence of the electric field [cf. (19)

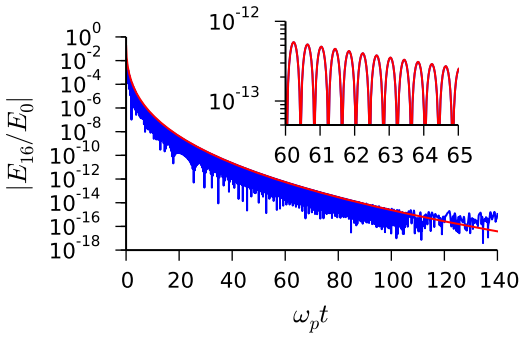


**Figure 13:** Electric field for $A = 0.1$, $kc/\omega_p = 8$ and $T/mc^2 = 0.2$ (blue) along with the amplitude given by (1) (red). The inset shows the electric field from the numerical solution (blue) along with a least-squares fit to (3); see Table 1.

in Sartori, 95]:

$$E \propto t^{1/6} \exp\left[-\frac{3\sqrt{3}}{4}\left(\mu^2 kc\,t\right)^{1/3}\right] \sin\left[kc\,t - \frac{3}{4}\left(\mu^2 kc\,t\right)^{1/3} + \frac{\pi}{12}\right]. \tag{2}$$

Comparing this to our numerical solution, we observe a phase error as can be seen in Fig. 12. To understand the origin of this discrepancy, we assume the time dependence derived by Sartori to be correct and attempt to fit the numerical solution to

$$E = C\,t^{1/6}\,e^{-p_1\,t^{1/3}} \sin\left(p_2\,t - p_3\,t^{1/3} + p_4\right). \tag{3}$$

The results of a least-squares fit (except for $C$ which is uninteresting) are shown in Table 1 along with the corresponding values from (2). Fig. 13 shows the electric field from the numerical solution and the result of fitting (3). We have repeated this procedure for different initial wavenumbers and equilibrium temperatures and in all cases we find the phase constant to be approximately $1.9$. These results strongly suggest that the constant phase in (1) is incorrect.

| | $p_1$ | $p_2$ | $p_3$ | $p_4$ |
|---|---|---|---|---|
| Fit | 7.54 | 7.94 | 4.39 | 1.92 |
| (19) of Sartori, 95 | 7.59 | 8.00 | 4.38 | 0.26 |

**Table 1:** Result of a least-squares fit the numerical solution to (3) compared the coefficients in (1). See Ref. [8].

# Supported Publications and Conference Presentations

### Refereed Publications

[1] B. M. Cowan, **S. Y. Kalmykov**, A. Beck, X. Davoine, K. Bunkers, A. F. Lifschitz, E. Lefebvre, D. L. Bruhwiler, **B. A. Shadwick**, and D. P. Umstadter, "Computationally Efficient Methods for Modelling Laser Wakefield Acceleration in the Blowout Regime," J. Plasma Phys. **78**, 469 (2012). http://dx.doi.org/10.1017/S0022377812000517

[2] S. Banerjee, **S. Y. Kalmykov**, N. D. Powers, G. Golovin, V. Ramanathan, N. J. Cunningham, K. J. Brown, S. Chen, I. Ghebregziabher, B. M. Cowan, D. L. Bruhwiler, A. Beck, E. Lefebvre, **B. A. Shadwick**, and D. P. Umstadter, "Stable, Tunable, Quasimonoenergetic Electron Beams Produced in a Laser Wakefield Near the Threshold for Self-injection," Phys. Rev. ST Accel. Beams **16**, 031302 (2013). http://dx.doi.org/10.1103/PhysRevSTAB.16.031302

[3] S. Y. Kalmykov, X. Davoine, and B. A. Shadwick, "All-Optical Control of Electron Self-Injection in Millimeter-Scale, Tapered Dense Plasmas," Nucl. Instrum. Methods in Phys. Res. A **740**, 266 (2014). http://dx.doi.org/10.1016/j.nima.2013.11.058

[4] A. Beck, **S. Y. Kalmykov**, X. Davoine, A. Lifschitz, **B. A. Shadwick**, V. Malka, and A. Specka, "Physical Processes at Work in sub-30 fs, PW Laser Pulse-Driven Plasma Accelerators: Towards GeV Electron Acceleration Experiments at CILEX Facility," Nucl. Instrum. Methods in Phys. Res. A **740**, 67 (2014). http://dx.doi.org/10.1016/j.nima.2013.11.003

[5] **B. A. Shadwick**, A. B. Stamm, and E. G. Evstatiev, "Variational Formulation of Macro-Particle Plasma Simulation Algorithms," Phys. Plasmas **21**, 055708 (2014). http://dx.doi.org/10.1063/1.4874338

[6] A. B. Stamm, **B. A. Shadwick**, and E. G. Evstatiev, "Variational Formulation of Macroparticle Models for Electromagnetic Plasma Simulations," IEEE Trans. Plasma Sci. **42**, 1747 (2014). http://dx.doi.org/10.1109/TPS.2014.2320461

[7] **S. Y. Kalmykov**, X. Davoine, R. Lehe, A. F. Lifschitz, and **B. A. Shadwick**, "Optical Control of Electron Phase Space in Plasma Accelerators with Incoherently Stacked Laser Pulses," Phys. Plasmas **22**, 056701 (2015). http://dx.doi.org/10.1063/1.4920962

[8] M. Carrié and **B. A. Shadwick**, "A Time-Implicit Numerical Method and Benchmarks for the Relativistic Vlasov–Ampere Equations," Phys. Plasmas **23**, 012102 (2016). http://dx.doi.org/10.1063/1.4938035

[9] **S. Y. Kalmykov**, X. Davoine, I. Ghebregziabher, R. Lehe, A. F. Lifschitz, and **B. A. Shadwick**, "Controlled Generation of Comb-Like Electron Beams in Plasma Channels for Polychromatic Inverse Thomson $\gamma$-Ray Sources," Plasma Phys. Control. Fusion **58**, 034006 (2016). http://dx.doi.org/10.1088/0741-3335/58/3/034006

[10] **S. Y. Kalmykov**, X. Davoine, I. A. Ghebregziabher, and **B. A. Shadwick**, "Customizable Electron Beams from Optically Controlled Laser Plasma Acceleration for $\gamma$-Ray Sources Based on Inverse Thomson Scattering.," Nucl. Instrum. Meth. A **829**, 52 (2016). http://dx.doi.org/10.1016/j.nima.2015.12.066

**Conference Proceedings**

[11] **S. Y. Kalmykov**, "Dark-Current-Free Laser-Plasma Acceleration in Blowout Regime Using Nonlinear Plasma Lens," in *AIP Conference Proceedings*, Vol. 1507 of *AIP Conference Proceedings*, edited by R. Zgadzaj, E. Gaul, and M. C. Downer (AIP, 2013), pp. 921–926. http://dx.doi.org/10.1063/1.4788989

[12] J. P. Reyes and **B. A. Shadwick**, "An Unconditionally-Stable Numerical Method for Laser-Plasma Interactions," in *Advanced Accelerator Concepts: Proceedings of the 15th Advanced Accelerator Concepts Workshop*, Vol. 1507 of *AIP Conference Proceedings*, edited by R. Zgadzaj, E. Gaul, and M. C. Downer (AIP, 2013), pp. 939–944. http://dx.doi.org/10.1063/1.4788992

[13] **S. Y. Kalmykov**, X. Davoine, and **B. A. Shadwick**, "Sub-Millimeter-Scale, 100-MeV-Class Quasi-Monoenergetic Laser Plasma Accelerator Based on All-Optical Control of Dark Current in the Blowout Regime," in *Advanced Accelerator Concepts: Proceedings of the 15th Advanced Accelerator Concepts Workshop*, Vol. 1507 of *AIP Conference Proceedings*, edited by R. Zgadzaj, E. Gaul, and M. C. Downer (AIP, 2013), pp. 289–294. http://dx.doi.org/10.1063/1.4773709

[14] B. M. Cowan, **S. Y. Kalmykov**, **B. A. Shadwick**, K. Bunkers, D. L. Bruhwiler, and D. P. Umstadter, "Improved Particle Statistics for Laser-Plasma Self-Injection Simulations," in *Advanced Accelerator Concepts: Proceedings of the 15th Advanced Accelerator Concepts Workshop*, Vol. 1507 of *AIP Conference Proceedings*, edited by R. Zgadzaj, E. Gaul, and M. C. Downer (AIP, 2012), pp. 375–380. http://dx.doi.org/10.1063/1.4773725

[15] F. M. Lee and **B. A. Shadwick**, "Modeling Asymmetric Beams Using Higher-Order Phase-Space Moments," in *Advanced Accelerator Concepts: Proceedings of the 15th Advanced Accelerator Concepts Workshop*, Vol. 1507 of *AIP Conference Proceedings*, edited by R. Zgadzaj, E. Gaul, and M. C. Downer (AIP, 2012), pp. 393–398. http://dx.doi.org/10.1063/1.4773728

[16] **S. Y. Kalmykov**, **B. A. Shadwick**, and X. Davoine, *All-optical control of electron trapping in plasma channels*, in 2013 19th IEEE Pulsed Power Conference (PPC), 1–6 (2013). http://dx.doi.org/10.1109/PPC.2013.6627518

[17] J. Paxon Reyes and **B. A. Shadwick**, *Higher-order explicit methods for laser-plasma interactions*, in 2013 19th IEEE Pulsed Power Conference (PPC), 1–5 (2013). http://dx.doi.org/10.1109/PPC.2013.6627594

[18] **S. Y. Kalmykov, B. A. Shadwick**, I. Ghebregziabher, X. Davoine, R. Lehe, A. F. Lifschitz, and V. Malka, "Accordion Effect in Plasma Channels: Generation of Tunable Comb-Like Electron Beams," in *Proceedings of the 41th IEEE International Conference on Plasma*

*Science and 20th International Conference on High-Power Particle Beams (ICOPS/BEAMS 2014)* (IEEE, 2014), pp. 1–6. http://dx.doi.org/10.1109/PLASMA.2014.7012740

[19] **S. Kalmykov**, **B. A. Shadwick**, and X. Davoine, "All-Optical Control of Electron Trapping in Plasma Channels," in *2013 19th IEEE Pulsed Power Conference*, San Francisco (2013), pp. 1–6, (http://dx.doi.org/10.1109/PPC.2013.6627518).

[20] **S. Y. Kalmykov**, X. Davoine, R. Lehe, A. F. Lifschitz, and **B. A. Shadwick**, "Accordion Effect Revisited: Generation of Comb-Like Electron Beams in Plasma Channels," in *Advanced Accelerator Concepts: Proceedings of the 16th Advanced Accelerator Concepts Workshop*, Vol. 1777 of *AIP Conference Proceedings*, edited by M. Hogan (AIP, 2016), p. 040007. http://dx.doi.org/10.1063/1.4965609

[21] **S. Y. Kalmykov**, I. A. Ghebregziabher, X. Davoine, R. Lehe, A. F. Lifschitz, V. Malka, and **B. A. Shadwick**, "Femtosecond Pulse Trains of Polychromatic Inverse Compton $\gamma$-Rays from Designer Electron Beams Produced by Laser-Plasma Acceleration in Plasma Channels," in *Advanced Accelerator Concepts: Proceedings of the 16th Advanced Accelerator Concepts Workshop*, Vol. 1777 of *AIP Conference Proceedings*, edited by M. Hogan (AIP, 2016), p. 080007. http://dx.doi.org/10.1063/1.4965664

[22] A. B. Stamm and **B. A. Shadwick**, "Variational Formulation of E & M Particle Simulation Algorithms in Cylindrical Geometry Using an Angular Modal Decomposition," in *Advanced Accelerator Concepts: Proceedings of the 16th Advanced Accelerator Concepts Workshop*, Vol. 1777 of *AIP Conference Proceedings*, edited by M. Hogan (AIP, 2016), p. 050004. http://dx.doi.org/10.1063/1.4965627

[23] **S. Y. Kalmykov**, X. Davoine, I. Ghebregziabher, and **B. A. Shadwick**, "Multi-Color $\gamma$-Rays from Comb-Like Electron Beams Driven by Incoherent Stacks of Laser Pulses," in *Advanced Accelerator Concepts: Proceedings of the 17th Advanced Accelerator Concepts Workshop*, *AIP Conference Proceedings*, edited by D. Gordon (AIP, 2016), in press.

**Invited Presentations**

[24] **B. A. Shadwick**, "Variational Formulation of Macro-Particle Algorithms for Kinetic Plasma Simulations," 2013 International Sherwood Fusion Theory Conference, Santa Fe, New Mexico, April 15–17, 2013.

[25] A. Stamm, "Variational Formulation of Particle Algorithms for Kinetic Electromagnetic Plasma Simulations", talk 10D-1, IEEE Pulsed Power & Plasma Science Conference PPPS 2013, San Francisco, California, June 16–21, 2013. http://dx.doi.org/10.1109/PLASMA.2013.6635213

[26] **B. A. Shadwick**, "A Variational Formulation of Macro-Particle Algorithms for Kinetic Plasma Simulations", talk JI2 5; Bull. Am. Phys. Soc. **58**, 144 (2013), 55th Annual Meeting of the APS Division of Plasma Physics. http://meetings.aps.org/link/BAPS.2013.DPP.JI2.5

[27] **S. Y. Kalmykov**, "Optical Control of Electron Trapping: Generation of Comb-Like Electron Beams for Tunable, Pulsed, Multi-Color Radiation Sources," Bull. Am. Phys. Soc. **59**, (2014), paper QI2.02, 56th Annual Meeting of the APS Division of Plasma Physics. http://meetings.aps.org/link/BAPS.2014.DPP.QI2.2

[28] **B. A. Shadwick**, 'Variational Formulation of Macro-Particle Algorithms for Kinetic Plasma Simulations," Joint Institute for Fusion Theory workshop on "Progress in Kinetic Plasma Simulations," New Orleans (November 2014).

[29] **S. Y. Kalmykov**, "Dark current and beam loading in the blowout regime of laser-plasma acceleration: A test-bed for reduced simulation methods," Joint Institute for Fusion Theory workshop on "Progress in Kinetic Plasma Simulations," New Orleans (November 2014).

**Contributed Conference Presentations**

**54th Annual Meeting of the APS Division of Plasma Physics**, Providence, Rhode Island, October 29–November 2, 2012

[30] **S. Y. Kalmykov**, B. A. Shadwick, and X. Davoine, "Ultracompact Quasi-Monoenergetic GeV-Scale Laser Plasma Accelerator Based on All-Optical Control of Dark Current in Longitudinally Tapered Plasmas," Bull. Am. Phys. Soc. 57(12) (2012) http://meetings.aps.org/link/BAPS.2012.DPP.PP8.113.

[31] **Jonathan Reyes** and B. A. Shadwick, "An Unconditionally-Stable Numerical Method for Laser-Plasma Interactions," Bull. Am. Phys. Soc. 57(12) (2012) http://meetings.aps.org/link/BAPS.2012.DPP.PP8.114.

[32] **Benjamin Cowan**, Serguei Kalmykov, Kyle Bunkers, John Cary, Brad Shadwick, and Donald Umstadter, "Improved Particle Statistics for Laser-Plasma Self-Injection Simulations," Bull. Am. Phys. Soc. **57** (12) (2012) http://meetings.aps.org/link/BAPS.2012.DPP.PP8.115.

[33] Michael Carrié and **B. A. Shadwick**, An Implicit Solver for the Vlasov–Poison Equation, Bull. Am. Phys. Soc. 57(12) (2012) http://meetings.aps.org/link/BAPS.2012.DPP.UP8.22.

**The 1st European Advanced Accelerator Concepts Workshop**, La Biodola, Isola d'Elba, Italy, June 2–7, 2013

[34] **S. Y. Kalmykov**, B. A. Shadwick, and X. Davoine, "All-Optical Control of Electron Injection for GeV-Scale Acceleration in mm-Scale, Tapered Plasmas."

**IEEE Pulsed Power & Plasma Science Conference PPPS 2013**, San Francisco, California, June 16–21, 2013

[35] **S. Y. Kalmykov**, X. Davoine, B. A. Shadwick, "All-Optical Control of Electron Trapping in Tapered Plasmas and Channels," talk 5C-1 http://www.npss-confs.org/ppps/program/GetPDFFile.asp?AID=1567.

[36] **B. A. Shadwick** and M. Carrié, "A Time-Implicit Algorithm for Solving the Vlasov–Poisson Equation," poster P4-12 http://www.npss-confs.org/ppps/program/GetPDFFile.asp?AID=1888.

[37] **J. P. Reyes** and B. A. Shadwick, "Higher-Order Explicit Numerical Methods for Laser-Plasma Interactions," poster P4-15 http://www.npss-confs.org/ppps/program/GetPDFFile.asp?AID=1877.

**19th IEEE Pulsed Power Conference and the 40th IEEE International Conference on Plasma Science**, San Francisco, June 16–21, 2013

[38] **S. Y. Kalmykov**, **B. A. Shadwick**, and X. Davoine, *All-Optical Control of Electron Trapping in Tapered Plasmas and Channels*. http://dx.doi.org/10.1109/PLASMA.2013.6633483

[39] J. Paxon Reyes and **B. A. Shadwick**, *Higher-Order Explicit Numerical Methods for Laser Plasma Interactions*. http://dx.doi.org/10.1109/PLASMA.2013.6634928

[40] B. A. Shadwick and M. Carrié *A Time-Implicit Algorithm for Solving the Vlasov–Poisson Equation*. http://dx.doi.org/10.1109/PLASMA.2013.6634925

**The 41st IEEE International Conference on Plasma Science and the 20th International Conference on High-Power Particle Beams**, Washington, May 25–29, 2014

[41] **S. Y. Kalmykov**, X. Davoine, **B. A. Shadwick**, *Optical Control of Electron Trapping and Acceleration in Plasma Channels: Application to Tunable, Pulsed Multicolor Radiation Sources*, talk 3C-4 http://ib14studenttravel.appspot.com/docs/program.pdf

**55th Annual Meeting of the APS Division of Plasma Physics**, Denver, November 11–15, 2013

[42] **S. Y. Kalmykov**, **B. A. Shadwick**, and X. Davoine, *All-Optical Control of Electron Trapping in Plasma Channels*, poster GP8 79; Bull. Am. Phys. Soc. **58**, 133 (2013). http://meetings.aps.org/link/BAPS.2013.DPP.GP8.79

[43] J. Paxon Reyes and **B. A. Shadwick**, *An Unconditionally-Stable Numerical Method for the Maxwell–Fluid Equations*, poster GP8 91; Bull. Am. Phys. Soc. **58**, 135 (2013). http://meetings.aps.org/link/BAPS.2013.DPP.GP8.91

[44] Alexander Stamm, **Bradley Shadwick**, and Evstati Evstatiev, *Variational Formulation of Particle Algorithms for Kinetic E & M Simulations*, poster CP8 53; Bull. Am. Phys. Soc. **58**, 83 (2013). http://meetings.aps.org/link/BAPS.2013.DPP.CP8.53

[45] **Bradley Shadwick** and Evstati Evstatiev, *Time-Discretized Action Principle Variational Formulation of Finite-Size Particle Simulation Methods for Electrostatic Plasmas*, poster CP8 59, Bull. Am. Phys. Soc. **58**, 84 (2013). http://meetings.aps.org/link/BAPS.2013.DPP.CP8.59

[46] Michael Carrié and **Bradley Shadwick**, *Solving the Vlasov-Poisson Equation and Preserving Positivity: Comparisons Between the Operator Splitting and Flux Limiting Method*, poster CP8 62; Bull. Am. Phys. Soc. **58**, 85 (2013). http://meetings.aps.org/link/BAPS.2013.DPP.CP8.62

**56th Annual Meeting of the APS Division of Plasma Physics**, New Orleans, October 27–31, 2014

[47] J. Paxon Reyes and **B. A. Shadwick**, "Discrete Variational Approach for Modeling Laser-Plasma Interactions," poster CP8.00052; Bull. Am. Phys. Soc. **59** (2014). http://meetings.aps.org/link/BAPS.2014.DPP.CP8.52

[48] Alexander Stamm and **B. A. Shadwick**, "A Variational Formulation of Particle Algorithms for Kinetic E&M Plasma Simulations in the Moving Window," poster JP8.00057; Bull. Am. Phys. Soc. **59** (2014). http://meetings.aps.org/link/BAPS.2014.DPP.JP8.57

[49] Michael Carrie and **B. A. Shadwick**, "Solving the 1D1P Relativistic Vlasov-Poisson System of Equations: Case Study of the Linear Landau Damping and Two-Stream Instability," poster JP8.00076; Bull. Am. Phys. Soc. **59** (2014). http://meetings.aps.org/link/BAPS.2014.DPP.JP8.76

**16th Advanced Accelerator Concepts Workshop**, San Jose, California, July 13-18, 2014

[50] **B. A. Shadwick**, "Variational Formulation of Macro-Particle Algorithms for Kinetic Plasma Simulation"

[51] **S. Y. Kalmykov**, "Accordion Effect in Plasma Channels: Generation of Designer Comb-Like Electron Beams for Advanced Radiation Sources"

[52] **S. Y. Kalmykov**, "Femtosecond Flashes of Multi-Color, MeV Inverse Compton Gamma-Rays from Designer e-Beams Produced by LPA in Plasma Channels"

[53] J. Reyes and **B. A. Shadwick**, "A Discrete Variational Approach for Modeling Laser-Plasma Interactions"

[54] Stamm and **B. A. Shadwick**, "A Variational Formulation of Particle Algorithms for Kinetic E&M Plasma Simulations"

**57th Annual Meeting of the APS Division of Plasma Physics**, Savannah, November 16–20, 2015

[55] **S. Y. Kalmykov**, **B. A. Shadwick**, I. Ghebregziabher, and X. Davoine, "Laser-Plasma Acceleration with Multi-Color Pulse Stacks: Designer Electron Beams for Advanced Radiation Sources," poster GP12.00004; Bull. Am. Phys. Soc. **60** (2015). http://meetings.aps.org/link/BAPS.2015.DPP.GP12.4

[56] J. Paxon Reyes and **B. A. Shadwick**, "Applying Boundary Conditions Using a Time-Dependent Lagrangian for Modeling Laser-Plasma Interactions," poster GP12.00025; Bull. Am. Phys. Soc. **60** (2015). http://meetings.aps.org/link/BAPS.2015.DPP.GP12.25

[57] Alexander Stamm and **B. A. Shadwick**, "Variational Formulation of Particle Algorithms for Kinetic E & M Plasma Simulations; A High Fidelity Approach," poster TP12.00048; Bull. Am. Phys. Soc. **60** (2015). http://meetings.aps.org/link/BAPS.2015.DPP.TP12.48

**17th Advanced Accelerator Concepts Workshop**, National Harbor, MD, July 31 – August 5, 2016

[58] **B. A. Shadwick**, "Deriving Numerical Models from Action Principles."

[59] J. Paxon Reyes and **B. A. Shadwick**, "Applying Boundary Conditions Using a Time-Dependent Lagrangian for Modeling Laser-Plasma Interactions."

[60] **S. Y. Kalmykov** and **B. A. Shadwick**, "Laser-accelerated comb-like electron beams as a source of pulsed polychromatic gamma-rays."

[61] A. B. Stamm, J. Palastro, D. Gordon and **B. A. Shadwick**,"Progress on Variational Formulations for Computational Modeling of Laser-Plasma Interactions."

**Completed Dissertations**

[62] A. B. Stamm, *Variational Formulation of Macro-Particle Algorithms for Studying Electromagnetic Plasmas*, Ph.D. thesis, University of Nebraska - Lincoln, 2015, paper AAI3738970. http://digitalcommons.unl.edu/dissertations/AAI3738970